TURBULENT HEAT TRANSFER IN NANOPARTICULATE MULTIPHASE CHANNEL FLOWS WITH A HIGH PRANDTL NUMBER MOLTEN SALT FLUID

B.H. MAHMOUD[1*], L.F. MORTIMER[1], M. COLOMBO[1], M. FAIRWEATHER[1], J. PEAKALL[2], H.P. RICE[1], D. HARBOTTLE[1]

[1]School of Chemical and Process Engineering, and [2]School of Earth and Environment, University of Leeds, Leeds LS2 9JT, UK
[*]bgy9bm@leeds.ac.uk

Abstract. The growing interest in energy efficient and sustainable technologies has created significant demand for novel heat transfer and thermal energy storage materials, such as nanofluids. The importance of nanoparticle science cannot be underestimated, since the motivation for the manipulation, through nanoparticle addition, of the properties of existing thermofluids (e.g. molten salt) arises from their poor thermal properties which represent a major limitation to the development of more energy-efficient processes. In this work, consideration is given to investigating the role of heat transfer in nanofluids in three-dimensional flows using an advanced computational modelling approach to simulate such flows. In the present work, we use direct numerical simulation coupled with a Lagrangian particle tracking technique. The heat transfer behaviour of a nanofluid within a turbulent wall-bounded flow is investigated, with the fluid phase properties chosen to represent a solar molten salt ($NaNO_3$-KNO_3, 60:40 weight ratio) thermofluid typical of those present in solar thermal power plants. The configuration is a fully developed channel flow with uniform heating/cooling from both walls. The continuous phase is modelled using the open source spectral element-based solver, Nek5000. Predictions of a statistically steady turbulent channel flow at shear Reynolds number $Re_\tau = 180$ and high turbulent Prandtl number $Pr_t = 5.0$ are first obtained and validated. A particle tracking routine is implemented to simulate the dispersed phase which can accommodate one-, two- and four-way coupling between the fluid and discrete phases. To investigate the effect of particles on the turbulent heat flux and temperature field, the nanoparticle concentration response to temperature variations and turbulence is obtained across the channel, with the associated first and second-order flow and temperature field statistics presented. The advantage of the model developed is its ability to study in detail phenomena such as interparticle collisions, agglomeration, turbophoresis and thermophoresis, with the approach also being of value in investigations of the heat transfer performance and long-term thermal stability of nanoparticle dispersions which as yet have not been considered in detail. The outcome of this study allows conclusions to be reached regarding the implications of nanoparticle-seeded molten salts for solar thermal energy storage systems.

1   INTRODUCTION

Particle-laden flows, containing micro-/nano-sized particulate (e.g. particles, colloids and surfactants) have gained increased attention recently because of their wide range of industrial

applications. Of particular interest are nanofluids, which are dilute fluid suspensions of nanoparticles (1-100 nm) at modest concentrations (< 5.0% weight fraction) [1]. They are prepared by dispersing nanoparticles in fluids such as water, oil, molten salt or ethylene glycol. Unlike conventional fluids, the significant enhancement of the thermal properties of molten salt containing nanoparticles allows new pathways for its high temperature application, particularly in the energy sector. In this sector, the efficiency of heat removal and thermal management systems is presently the greatest technological challenge. The use of molten salt nanofluids as a heat transfer fluid and energy storage medium for power generation and storage is very promising and could result in increased efficiency and large energy savings [2]. The flow and heat transfer of such nanofluids is therefore gaining a lot of interest by researchers in the academic community due to their inherent improved thermal transport properties.

Understanding of the hydrodynamics, heat transfer and thermal enhancement of molten salt nanofluids is quite challenging if it is to be gained only experimentally. Apart from the restrictions of size and harsh environmental (i.e. high temperature differences), many other complications arise from the responsible hydrodynamic and interaction forces which are likely to take place at varied magnitudes and multiple time scales. The use of a numerical approach is therefore proposed to investigate these phenomena. More specifically, it is intended here to develop a multiscale computational model based on Lagrangian particle tracking (LPT) [3] coupled with direct numerical simulation (DNS) to investigate the dispersion stability, thermal properties and turbulent heat flux in nanofluids in a channel flow. The other benefit of this computational fluid dynamic (CFD) model is its ability to investigate more intrinsic phenomena such as turbophoresis (the tendency for particles to migrate in the direction of decreasing turbulence kinetic energy) and thermophoresis (particle motion induced by thermal gradients), and hence the long-term thermal stability of nanofluids that has not yet been well studied.

It is thought that agglomeration of nanoparticles to form larger particle clusters could lead to surface impact, deposition and erosion, although evidence of this in the literature is conflicting [4], with few quantitative studies reported. To capture these effects using CFD, a comprehensive description of both the fluid phase and solid nanoparticle phase evolution is necessary. Since these particles are very small, with Stokes numbers St ~ 0, they are expected to behave like tracers within the carrier phase. Hence, the focus here is on the fluid phase that dictates the spatial distribution of solid particles relative to the turbulent flow. The evolution of the particles' distribution is therefore highly dependent on the turbulent flow and temperature fields, and physical interactions between the particles and between the particle and the cold or hot wall heat flux boundaries. Moreover, whereas most transport models are not explicit and do not account for feedback between the turbulence and aggregation mechanisms, the model proposed does so.

2 METHODOLOGY

The focus of the present DNS-based work relies on modelling the heat transfer in nanoparticulate multiphase channel flows with a high Prandtl number fluid (i.e. molten salt). The method proposed uses a channel flow configuration in three-dimensions that is used to simulate turbulent flows representative of those encountered in practice by providing a full range of length and time scales, down to the Kolmogorov scale [5]. This technique enables any quantity of interest to be analysed with great spatial and temporal precision, albeit at a large

computational cost and for somewhat idealised conditions. DNS can generally be regarded as a complement to laboratory experiments. Particle-particle interactions are represented using detailed surface interactions based on DLVO interaction forces [6]. DLVO theory (after Derjaguin and Landau [7], and Verwey and Overbeek [8]) defines inter-particle forces as the sum of van der Waals and electric double-layer contributions, and these are fully resolved in the computations.

Turbulent heat transfer in a channel is characterized not only by the Reynolds number (Re) but also by the Prandtl number (Pr) of the fluids. Kawamura et al. [9] undertook DNS simulations of turbulent heat transfer for various Prandtl numbers ranging from Pr = 0.025 to 5 with a Re_τ = 180 flow using a finite-difference method-based solver. They assumed a constant volumetric heating with a uniform wall temperature. Profiles of the mean temperature, temperature variance and turbulent heat flux were obtained, with detailed budgets within the transport equations for these quantities reported. The present work utilizes a similar turbulent heat transfer model to that of Kawamura et al. [9]. However, we here aim to expand on this work by seeding the continuous phase with nanoparticles to determine turbulence quantities such as the turbulent heat flux and temperature variance of the multiphase system considered with Pr = 5 and Re_τ = 180.

In order to relate the present work to the systems present in solar thermal power plants, we consider mechanical and chemical properties matching those of Al_2O_3 nanoparticles in molten salt ($NaNO_3$-KNO_3, 60-40 weight ratio), which is a simulant for proposed heat transfer fluid and thermal energy storage media. In addition, a novel method is used here to describe the oscillating layered structure of molten salt fluids (represented by the matrix of liquid molecules around the nanoparticles), and the influence of the interfacial layer thickness on the system conductivity. Further details can be found elsewhere [10]. This innovative approach allows for the simulation of different flows, and modifications to them to gain a better understanding of the nanoparticle dynamics and heat transfer characteristics of the system. The final outcome is expected to provide the optimum characteristics of the nanofluid flows that can be used in solar power plants.

2.1 Fluid flow simulation

In the present study the simulations were performed using a numerical multiscale model with the continuous phase predicted using the open source spectral element-based DNS code, Nek5000 [11]. This code was chosen based on its extensive testing, efficient parallelization capabilities and validation history [12]. Within the code, the incompressible Navier-Stokes equations (mass and momentum conservation) are solved to high accuracy, with the code applied to a Cartesian grid consisting of 27×18×23 8th order elements (i.e. 5.7 M nodes) used to represent a turbulent channel flow at shear Reynolds number Re_τ = 180 (equivalent to a bulk Reynolds number Re_B = 2800). A constant fluid timestep of Δt_F^* = 0.01 was used throughout. The elements were scaled such that those closest to the wall were distributed more densely. The geometry of the channel was 14δ×2δ×6δ, with δ = 0.1 mm, as illustrated in Fig. 1. For the purpose of this study, the computational coordinates (x, y, z) were used to represent the three-dimensional geometry of the channel, with x being the streamwise direction, y the wall-normal direction, and z the spanwise direction. Periodic boundary conditions were enforced in the streamwise and spanwise directions, while the wall-normal axis used solid impenetrable no-slip

conditions at $y^* = \pm\delta$, with the walls maintained at a constant temperature. The flow was driven and maintained by a constant pressure gradient. The non-dimensional Navier-Stokes equations are presented in Eqs. (1) and (2), with distances, velocities and densities normalized by the channel half-height, δ, the bulk velocity, U_B, and the fluid phase density, ρ_F, respectively. From here on, any quantity with an asterisk (*) denotes a variable non-dimensionalised in this manner.

$$\boldsymbol{\nabla} \cdot \boldsymbol{u}^* = 0 \tag{1}$$

$$\frac{\partial \boldsymbol{u}^*}{\partial t^*} + \boldsymbol{u}^* \cdot \boldsymbol{\nabla}\boldsymbol{u}^* = -\boldsymbol{\nabla}p^* + \frac{1}{Re_B}\boldsymbol{\nabla}\cdot\boldsymbol{\tau}^* + \boldsymbol{f}c \tag{2}$$

Here, $\boldsymbol{u}^*$ is the fluid velocity, p^* is the fluid pressure, Re_B is the bulk Reynolds number defined as $Re_B = U_B\delta/\nu_F$, ν_F is the fluid kinematic viscosity and $\boldsymbol{\tau}^*$ is the viscous stress tensor. The additional term $\boldsymbol{f}c$ is cell-dependent and accounts for two-way momentum exchange between particles in a cell and the surrounding fluid. The flow is driven and maintained by a constant pressure gradient using the following parameters:

$$\frac{\partial p}{\partial x} = \left(\frac{Re_\tau}{Re_B}\right)^2 \tag{3}$$

where Re_τ and Re_B are the shear and bulk Reynolds numbers, respectively.
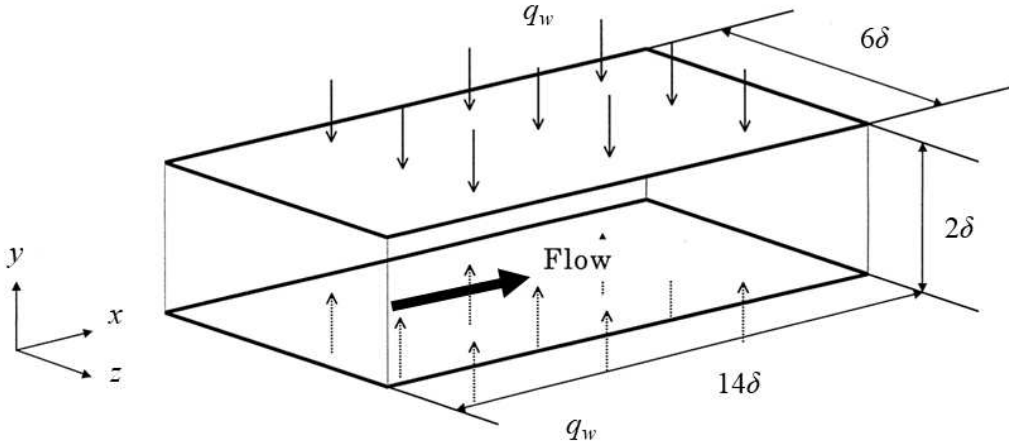

Figure 1: Configuration of DNS for turbulent heat transfer channel flow for hot wall case. Direction of q_W is reversed for cold wall case.

In addition to the fluid flow, Nek5000 also solves the following non-dimensional conservation equation for energy transport:

$$\frac{\partial T^*}{\partial t^*} + \mathbf{u}^* \cdot \nabla T^* = \frac{1}{Pe}\nabla \cdot \nabla T^* + q_{vol} \tag{4}$$

4

where T^* is the temperature, q_{vol} is the volumetric heat source term and $Pe = LU/\alpha$ with $\alpha = k/\rho_F C_p$, in which Pe is the Péclet number, L is a characteristic length, U the local flow velocity, k the thermal conductivity, ρ_F the fluid density, and C_p the heat capacity.

Two simulations were performed using Eq. (4) with different heat flux boundary conditions. The first had a fixed cold wall boundary with an associated temperature of 250 °C, whereas the second was set to have a fixed hot wall boundary with an associated temperature of 500 °C. The fluid used in these simulations was set to have a high Prandtl number (Pr = 5), representative of molten salt at 400 °C.

2.2 Dispersed phase simulation

The dispersed phase was represented by 500k, 100 nm diameter Al_2O_3 particles which were tracked through the fluid flow field. These were simulated using a Lagrangian particle tracking routine, which was developed for this work and implemented to interface concurrently with Nek5000. The motion of each nanoparticle is described using the Langevin equation, where the translational velocity of the i-th particle is obtained from the principle of conservation of linear momentum using:

$$m_p \frac{\partial \boldsymbol{v}_i}{\partial t} = \boldsymbol{F}_i \tag{4}$$

where

$$\boldsymbol{F_i} = \boldsymbol{F}_i^C + \boldsymbol{F}_i^e + \boldsymbol{F}_i^V + \boldsymbol{F}_i^f + \boldsymbol{F}_i^B \tag{5}$$

Here, m_p and $\boldsymbol{v}_i$ are the mass and the transitional velocity vector of the i-th nanoparticle, respectively. $\boldsymbol{F}_i^C$ is the particle contact force, $\boldsymbol{F}_i^e$ is the electric double layer repulsive force, $\boldsymbol{F}_i^v$ is the van der Waals attractive force, $\boldsymbol{F}_i^f$ is the fluid force and $\boldsymbol{F}_i^B$ is the random Brownian motion force. Other body forces such as gravity and buoyancy were found to be negligible for all length and time scales, since their magnitudes are much smaller than the aforementioned hydrodynamic and interaction forces . At each timestep, the motion of each particle was calculated accounting for the various forces noted. The temperature dependence of these force terms was obtained by interpolating the temperature field at the position of the particle, i.e. it was assumed that each nanoparticle had a temperature equal to that of the local fluid. Further details can be found elsewhere [3].

The model described was used to simulate the dynamics and mechanisms responsible for nanoparticle dispersion and aggregation, and was fully coupled (i.e. four-way coupled). Consideration of solely fluid forces acting upon the particulate phase is known as one-way coupling. Two-way coupling was achieved by implementing the point-source-in-cell method whereby particle forces were fed back to the local fluid cells. Particle collisions (four-way coupling) were resolved using the soft sphere approach, as described by Hertzian normal contact theory [13]. Finally, four-way coupled predictions were extended to include DLVO interparticle van der Waals attractive and electric double layer repulsive forces to allow the prediction of particle-particle agglomeration events [3]. Chemical and mechanical properties were chosen to match Al_2O_3 in molten salt, with the parameters used in the simulations provided in Table 1.

Table 1: Parameters used in the simulations.

Parameter	Carrier phase (NaNO$_3$-KNO$_3$)	Particle phase (Al$_2$O$_3$)
Shear Reynolds number, Re$_\tau$	180	-
Bulk Reynolds number, Re$_B$	2800	-
Particle diameter, d$_p$ / nm	-	100
Number of particles, N$_p$	-	500,000
Volume, V / m^3	1.58×10^{-10}	4.07×10^{-13}
Volume fraction, Φ / vol %	-	0.26
Temperature, T / °C	420	420
Bulk velocity, U$_B$ / m s^{-1}	25.67	25.68
Density, ρ / kg m^{-3}	1996.5	3850
Kinematic viscosity, ν_F / m^2 s^{-1}	0.974×10^{-6}	-

The simulations were first performed as an unladen single-phase molten salt flow using an arbitrary initial turbulence profile with added chaotic terms in the wall-normal and spanwise directions. Once turbulence was established, fluid statistics were monitored every 1500 timesteps until the mean and fluctuating velocity and temperature fields reached a statistically steady state. Particles were then injected uniformly throughout the channel and given an initial velocity equal to that of the local fluid. Particle statistics in the wall-normal direction were obtained by splitting the domain into 120 equal volume cuboidal regions, and by averaging over all particles within each region. From this steady state condition, four-way coupled runs were started, reducing the fluid and particle time step initially to avoid divergences in the flow field due to the impact of particle forces. The statistics obtained in these runs are presented and discussed in the following section.
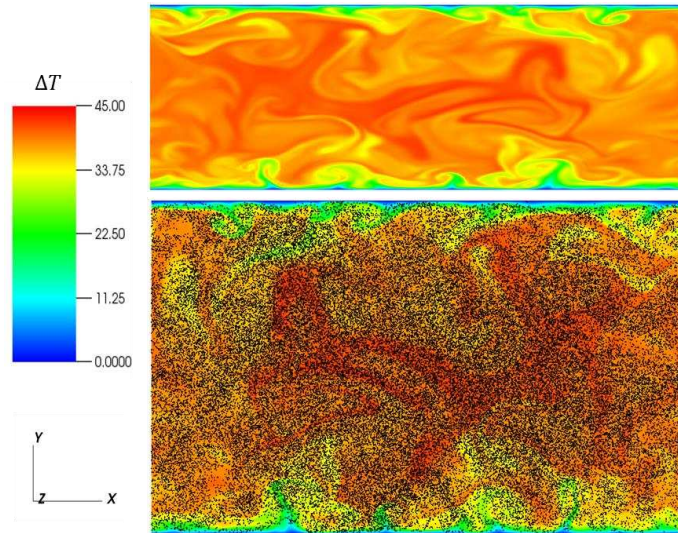
Figure 2: Instantaneous temperature distribution in unladen flow (top), and a zoomed in portion with nanoparticles for the hot wall case (bottom).

6

3 RESULTS AND DISCUSSION

3.1 Single-phase flow statistics

The results of each simulation were analysed to explain the flow and heat flux behaviour of the fluid and the nanoparticles within the channel. Figure 2 shows the instantaneous fluid temperature at the top of the figure, as well as illustrating the location of the nanoparticles in a zoomed in portion of the channel with hot walls in the lower part of the figure. Considering the results of Fig. 2, a trend in preferential concentration of particles within the coldest regions is noticeable. It is also evident that the particles exhibit increased concentrations in the centre of the channel. The reasons for this will be discussed later.
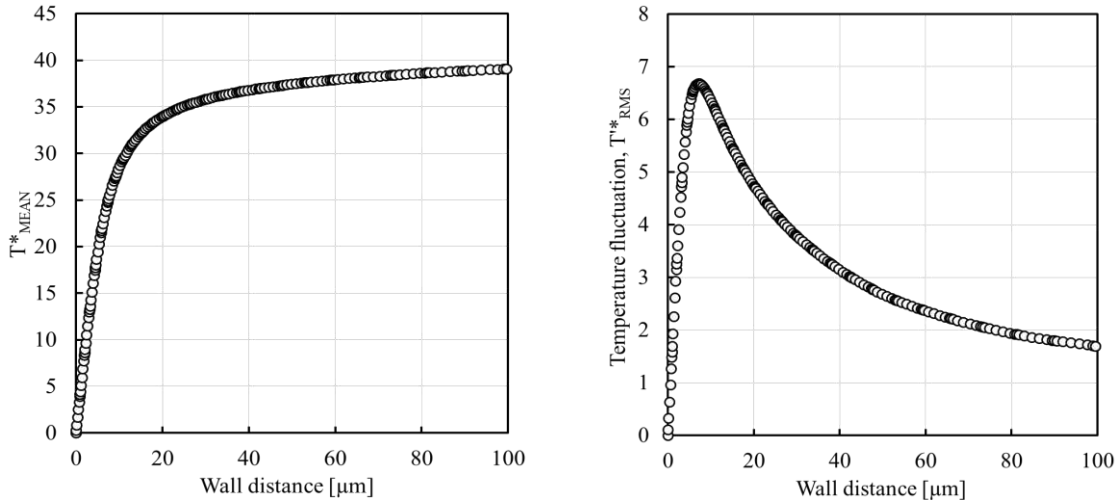

Figure 3: Mean temperature profile (left), and root-mean-square of temperature fluctuations (right).
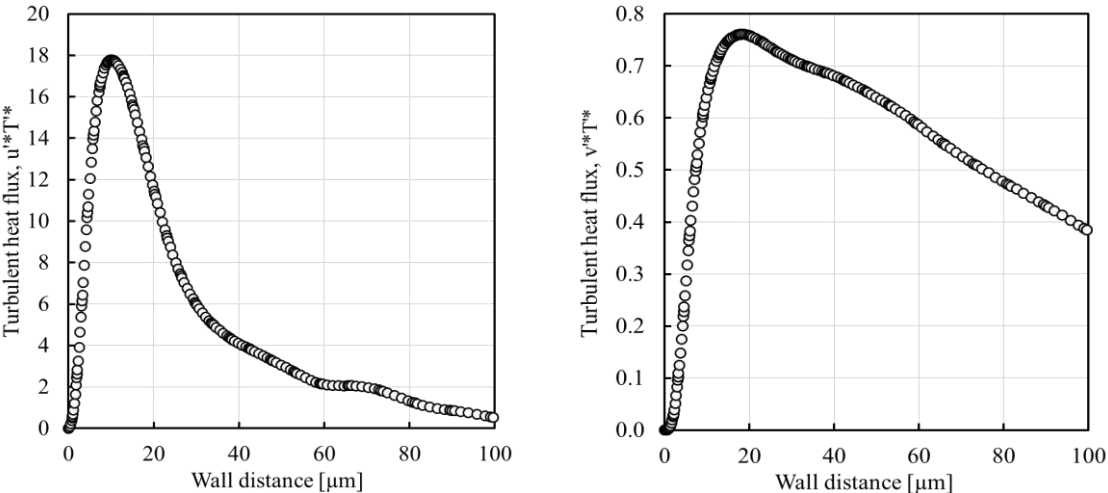

Figure 4: Turbulent heat flux components: streamwise (left) and spanwise (right).

Profiles of the mean temperature and root-mean-square (rms) of temperature fluctuations are presented in Fig. 3 for the single-phase flow. The statistics of Kawamura et al.'s [8] DNS of

turbulent heat transfer in a channel flow at $Re_\tau = 180$ and Prandtl number $Pr = 5$ were used for comparison and found to be in qualitatively good agreement. Small discrepancies were apparent between the two set of results, but these may be attributed to be a consequence of computational issues due to differences in the number of nodes and elements used in each simulation, with the present work using an order of magnitude higher number of nodes.

The turbulent heat fluxes in the streamwise and spanwise directions are also presented in Fig. 4. These determine the rate and direction of heat energy transfer via turbulence either towards (cold wall) or away from (hot wall) the wall.

3.2 Particle-laden flow statistics

Profiles of the streamwise mean particle velocity and the rms of particle streamwise velocity fluctuations are shown in Fig. 5.
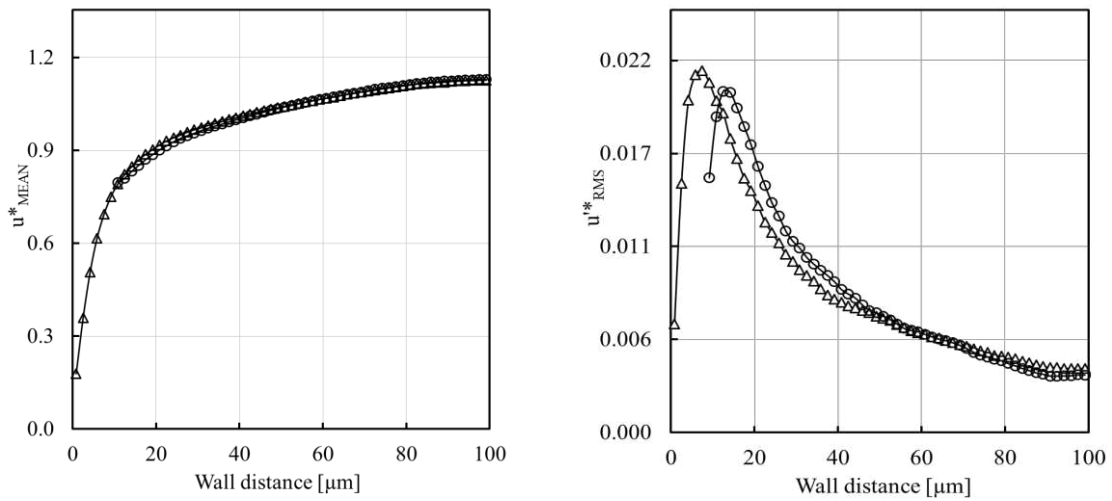

Figure 5: Streamwise mean particle velocity profiles (left), and root-mean-square of streamwise particle velocity fluctuations (right) – ○: hot wall; △: cold wall.

It is clear that the streamwise mean particle velocity distributions are similar for both the cold and hot wall configurations. This is likely due to the low particle Stokes number and the lack of dependence of mean streamwise flow behaviour on the temperature field. In the case of the hot wall, the statistics near the wall are not plotted due to insufficient particles in these regions to obtain meaningful averages. However, the rms of velocity fluctuation profiles show variation between the two configurations. In the case of the cold wall, the peak is closer to the wall, indicating that the particles behave in a more turbulent fashion within the near-wall region. This is likely to be due to thermophoresis causing a drift in the wall-normal direction towards the wall. For the hot wall case, the peak particle rms value is reduced and shifted towards the channel centre slightly, since particles which approach the wall are encouraged to move away from it due to increased local temperatures, although the spread of streamwise rms velocities further from the wall is maintained. The rms of velocity fluctuations in the wall-normal and spanwise directions is illustrated in Fig. 6. It can be seen that the wall-normal particle fluctuations exhibit similar behaviour near the wall, but the fluctuations are slightly increased for the cold wall

configuration in the outer layer. This is likely to be due to turbophoresis and thermophoresis working together to give the particles greater distributions in wall-normal velocity. The spanwise distributions exhibit similar behaviour, as expected since this direction is homogeneous in both fluid temperature and velocity distributions.
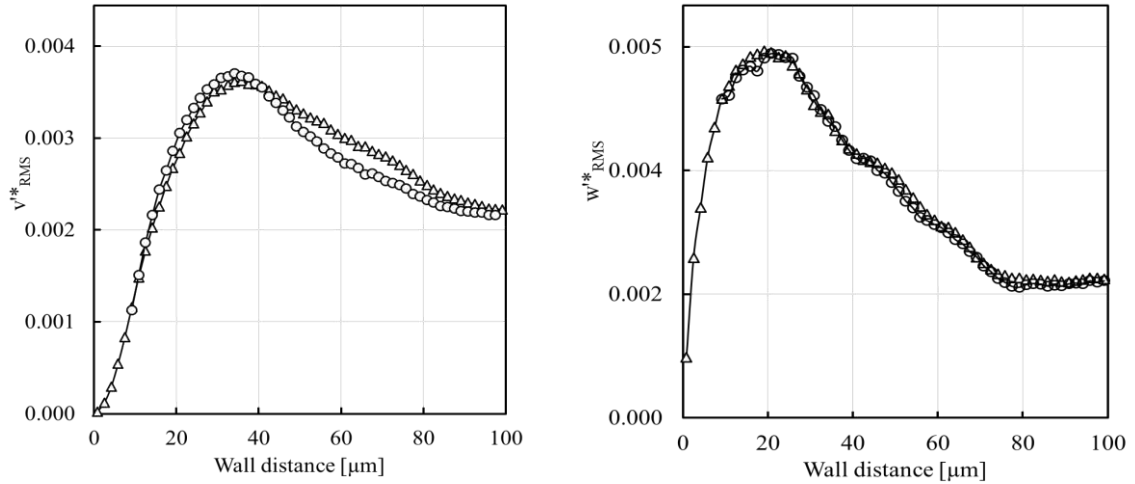

Figure 6: Root-mean-square of particle velocity fluctuations, wall-normal (left) and spanwise (right) – ○: hot wall; △: cold wall.
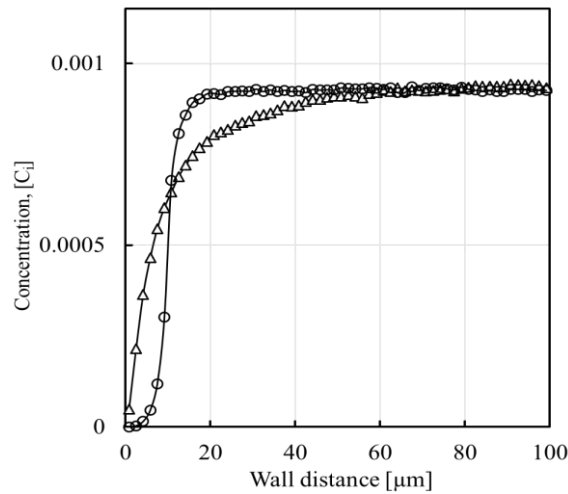

Figure 7: Comparison of mean particle concentrations across the channel – ○: hot wall; △: cold wall.

The predictions also demonstrate how particle concentrations differ in the near-wall regions due to thermophoresis, as illustrated in Fig. 7. Over the course of the cold wall simulation it is clear that both turbophoresis and thermophoresis take place, encouraging the particles to migrate to regions of low turbulence kinetic energy and temperature (i.e. near the walls). Over time this leads to a build-up of nano-particulate concentrations close to the wall. This has implications for particle collision and agglomeration rates since the local concentration in these regions is greater than the initial concentration once the system has reached a steady state. This also implies that, with time, particle deposition rates on the walls will likely increase due to

9

migration towards the walls. Conversely, the results for the hot wall boundary condition show particles are migrating away from the walls towards the channel centre. The preferential concentration of particles within the hottest zones of the channel in this case was also noted previously through the observations in regards to the results of Fig 2.

4 CONCLUSIONS

Direct numerical simulations of turbulent nanofluid flow and heat transfer were performed for two different thermal wall configurations (cold and hot walls) using a high Prandtl number fluid, and the effect on nanoparticle motion statistical quantities was investigated. Concentration plots indicate a notable difference in particle distributions between the cold and hot wall boundary conditions. Specifically, it was observed that an increase in particle concentration in the near-wall regions occurred over the run times considered for the cold wall configuration. The particles were found to behave in a more turbulent fashion in the near-wall regions, due to thermophoresis causing a drift in the wall-normal direction towards the wall. Combined turbophoresis and thermophoresis effects were also found to give the particles larger distributions in the wall-normal velocity. For the hot wall case, particle migration was observed to be in the opposite direction, away from both of the walls towards the channel centre, as particles that approach the wall are encouraged away due to the increased wall temperature. The results obtained highlight differences in particle migration due to the wall temperature boundary condition, which over time will lead to a build-up of a non-homogeneous particulate concentrations within the channel. Future work will further consider the influence of turbophoresis and thermophoresis in more detail, and will allow conclusions to be reached regarding the implications for thermal energy storage systems using nanofluids.

5 ACKNOWLEDGEMENTS

REFERENCES

[1] Choi, S.U.S. and Eastman, J.A. Enhancing thermal conductivity of fluids with nanoparticles. Developments and Applications of Non-Newtonian Flows, ASME, New York, FED-Vol 231/MD-Vol 66, 99-105 (1995).

[2] Lenert, A. and Wang, E.N. Optimization of nanofluid volumetric receivers for solar thermal energy conversion. Sol. Energy (2012) **86**:253-265.

[3] Mahmoud, B.H., Fairweather, M., Mortimer, L.F., Peakall, J., Rice, H.P. and Harbottle, D. Prediction of stability and thermal conductivity of nanofluids for thermal energy storage applications. 28th European Symposium on Computer Aided Process Engineering (2018) **43**:61-66.

[4] Nguyen, C., Galanis, N., Polidori, G., Fohanno, S., Popa, C. and Bechec, A. An experimental study of a confined and submerged impinging jet heat transfer using Al_2O_3-water nanofluid. Int. J. Therm. Sci. (2009) **48**:401-411.

[5] Mortimer, L.F., Njobuenwu, D.O. and Fairweather, M. Near-wall dynamics of inertial particles in dilute turbulent channel flows. Phys. Fluids (2019) **31**:063302.

[6] Henry, C., Minier, J.P., Pozorski, J. and Lefèvre, G. A new stochastic approach for the simulation of agglomeration between colloidal particles. Langmuir (2013) **29**:13694-13707.

[7] Derjaguin, B. and Landau, L. Theory of the stability of strongly charged lyophobic sols and of the adhesion of strongly charged particles in solutions of electrolytes. Acta Physicochim. (1941) **14**:633-662.

[8] Verwey, E.J.W. and Overbeek, J.T.G. Theory of the stability of lyophobic colloids. J. Colloid Sci. (1955) **10**:224-225.

[9] Kawamura, H., Ohsaka, K., Abe, H. and Yamamoto, K. DNS of turbulent heat transfer in channel flow with low to medium-high Prandtl number fluid. Int. J. Heat and Fluid Flow (1998) **19**:482-491.

[10] Mahmoud B.H., Mortimer L.F., Fairweather, M., Rice, H.P., Peakall, J. and Harbottle D. Thermal conductivity prediction of molten salt-based nanofluids for energy storage applications. 29th European Symposium on Computer Aided Process Engineering (2019) **46**:601-606.

[11] Fischer, P.F., Lottes, J.W. and Kerkemeier, S.G. Nek5000, http://nek5000.mcs. anl.gov, (2008).

[12] Mahmoud B.H., Mortimer, L.F., Fairweather, M., Rice, H.P., Peakall, J. and Harbottle, D. Nanoparticle behaviour in multiphase turbulent channel flow. 29th European Symposium on Computer Aided Process Engineering (2019) **46**:607-612.

[13] Timoshenko, S. P. and Goodier, J.N. Theory of Elasticity. McGraw-Hill, New York, 3rd Ed., (1970).